Materials Advances

ROYAL SOCIETY OF CHEMISTRY

PAPER

View Article Online
View Journal | View Issue

Cite this: *Mater. Adv.*, 2021, **2**, 1676

Preparation and characterization of sodium-ion conductive Na_3BS_3 glass and glass–ceramic electrolytes†

Fumika Tsuji,[a] Akira Nasu,[a] Chie Hotehama,[a] Atsushi Sakuda,[a] Masahiro Tatsumisago[a] and Akitoshi Hayashi *[ab]

In order to find suitable solid electrolytes for all-solid-state sodium batteries, sulfide electrolytes composed of tetrahedral structural units such as PS_4, SnS_4 and SbS_4 have been widely studied. In this paper, the ionic conductivities of Na_3BS_3 *ortho*-thioborate electrolytes with triangular BS_3 units are firstly reported. Na_3BS_3 glass was prepared *via* a mechanochemical process from crystalline Na_3BS_3 (monoclinic phase). The crystalline Na_3BS_3 was pre-synthesized from a mixture of Na_2S, B, and S due to the instability of the B_2S_3 compound. A new metastable phase of trigonal Na_3BS_3 was precipitated as the primary phase by crystallization of the Na_3BS_3 glass. The prepared glass–ceramic electrolyte showed a higher ionic conductivity than the monoclinic Na_3BS_3 phase. The Na_3BS_3 glass showed the highest conductivity of 1.1×10^{-5} S cm^{-1}, which was higher than that of conventional Na_3PS_4 glass. Futhermore, the Na_3BS_3 glass showed a superior formability and electrochemical stability to $Na_{15}Sn_4$ negative electrode. An all-solid-state cell with the Na_3BS_3 glass as an electrolyte successfully operated as a secondary battery at 60 °C. It is concluded that the Na_3BS_3 glass with triangular structural units has appropriate properties as a solid electrolyte for application to all-solid-state sodium batteries. The results of this study extend research on multi-component sulfide electrolytes with triangular BS_3 structural units and contribute to the development of solid electrolytes for all-solid-state batteries.

Received 9th October 2020,
Accepted 31st January 2021

DOI: 10.1039/d0ma00777c

rsc.li/materials-advances

1. Introduction

Sodium-ion batteries with their associated low costs and abundant sodium reserves have attracted significant attention as promising next-generation large-scale energy storage systems to replace lithium-ion batteries. Because sodium has a similar electrochemical performance to lithium, such as standard reduction potential, sodium batteries have the potential to exhibit a high performance.[1–3] As one example of sodium-ion batteries, sodium–sulfur batteries can function as a stationary storage system. However, they require a high temperature of over 300 °C to operate with their molten electrodes, which causes cost and safety concerns.[4] To overcome these issues, all-solid-state sodium–sulfur batteries operated at room temperature are desirable. This requires superior solid electrolytes with high ionic conductivities at room temperature and good formabilities for achieving large contact areas with electrode active materials.

We previously reported that Na_3PS_4 glass–ceramics in a metastable cubic phase obtained *via* a mechanochemical process and consecutive heat treatment exhibited a higher ionic conductivity than crystalline Na_3PS_4 in the tetragonal phase.[5] The Na_3PS_4 sulfide system possesses a better formability than the Li_3PS_4 system, and its densification and associated sintering behavior are easily promoted by pressing at room temperature.[6] Subsequently, some sodium sulfides, such as Na_3SbS_4 and $Na_{11}Sn_2PS_{12}$, have been found to exhibit high ionic conductivities of over 1 mS cm^{-1} at room temperature.[7–11] In particular, we reported a $Na_{2.88}Sb_{0.88}W_{0.12}S_4$ glass–ceramic electrolyte with the highest ionic conductivity of 32 mS cm^{-1} among sulfide lithium and sodium-ion conductors reported so far.[12]

Studies on solid electrolytes have thus far focused on sulfide systems with tetrahedral structure units, such as PS_4^{3-} and SbS_4^{3-}. In contrast, solid electrolytes composed of triangular structural units have not been extensively studied. Solid electrolytes containing B as a center element are known to have triangular boron units in the systems of Na_2O–B_2O_3 and Na_2S–B_2S_3. We reported the preparation of Na_3BO_3 orthoborate glass

[a] *Department of Applied Chemistry, Graduate School of Engineering, Osaka Prefecture University, 1-1, Naka-ku, Sakai, Osaka 599-8531, Japan. E-mail: hayashi@chem.osakafu-u.ac.jp*
[b] *Elements Strategy Initiative for Catalysts and Batteries Kyoto University, Kyoto University, Sakyo, Kyoto 606-8501, Japan*

† Electronic supplementary information (ESI) available. See DOI: 10.1039/d0ma00777c

with a triangular BO_3^{3-} unit *via* a mechanochemical process, and its ionic conductivity was over 10^{-8} S cm^{-1}.[13] In general, the sodium-ion conductivity of glassy electrolytes increases with increasing Na content. The conductivities of Na_2S–B_2S_3 glasses prepared by conventional melt quenching have only been investigated for compositions with less than 67 mol% Na_2S,[14] while the conductivities of Na_3BS_3 *ortho*-thioborate glasses with Na content higher than 75 mol% Na_2S have not been reported. Another challenge for developing the sodium thioborate system is the difficulty in obtaining pure B_2S_3, which is not commercially available. Although the synthesis of B_2S_3 has been reported,[15] it is generally difficult to obtain pure B_2S_3 due to its low chemical stability and tendency to easily oxidation.

In this study, Na_3BS_3 sulfide electrolytes with three-coordinated borons were synthesized directly from a starting mixture of Na_2S, B, and S reagents. Crystalline Na_3BS_3 (monoclinic phase) was prepared by a solid-phase reaction in advance, which was then used to prepare glassy Na_3BS_3 *via* a mechanochemical process. A metastable crystalline phase was precipitated by crystallization of the prepared glassy Na_3BS_3. The structure and ionic conductivity of the prepared Na_3BS_3 electrolytes were examined, and their application to all-solid-state sodium cells was investigated.

2. Experimental

A mixture of Na_2S (>99.1%; Nagao), crystalline B (>99%; Kojundo Chem.), and S (>99.99%; Kojundo Chem.) was pelletized and placed into a carbon crucible, then heated at 700 °C for 10 h in a quartz ampoule sealed under vacuum. After cooling to room temperature slowly, crystalline Na_3BS_3 was obtained. The Na_3BS_3 glass was prepared from the crystalline Na_3BS_3 by a mechanochemical technique at an ambient temperature using a planetary ball mill (Pulverisette 7; Fritsch) with zirconia pots (45 mL in volume) and zirconia balls (4 mm in diameter, 45 g). The total mass of the starting materials was 0.4 g in each pot, and the rotational speed and milling duration were 310 rpm and 50 h, respectively. The milled sample powders were then heated in an electric furnace at 200 or 300 °C for 1 h. The heating temperatures were determined *via* differential thermal analysis (DTA). All processes were performed in a dry Ar atmosphere.

X-ray diffraction (XRD) measurements of the prepared materials were performed using CuKα radiation with a diffractometer (SmartLab; Rigaku). The diffraction data were collected in steps of 0.01° in the 2θ range of 10.0°–80.0°. The XRD measurements were performed using an airtight vessel with a beryllium window to prevent exposure of the sample to the air. The crystalline structures were refined using the SLS2 software (Rigaku), and the heated sample patterns were refined using the Rietveld method in the software package RIETAN-FP.[16]

^{11}B solid-state NMR experiments were performed using an NMR spectrometer (JNM-ECX 400; JEOL). The sample powders were packed into zirconia spinners in a dry Ar atmosphere. The observation frequency was 128.3 MHz. The spectra were acquired using a single pulse with a pulse width of 1.17 μs (1/3 of 90° pulse width), a recycle pulse delay of 0.5 s, and an MAS rate of 12 kHz. The chemical shifts were calibrated using BPO_4 (−3.6 ppm).

Raman spectra of the samples were measured using a Raman spectrophotometer (LabRAM HR-800; Horiba) with a 532 nm solid-state laser to identify the structural units. The electrolyte samples were placed in an airtight vessel with a quartz window. The process was performed in a dry Ar atmosphere.

DTA was performed using a thermal analyzer (Thermo Plus TG8110; Rigaku) at a heating rate of 10 °C min^{-1} under N_2 gas. The milled samples were sealed in Al pans in a dry Ar atmosphere.

The ionic conductivities were determined *via* AC impedance measurements using an impedance analyzer (Solartron; 1260) in the frequency range from 10 Hz to 1 MHz with an applied AC voltage of 50 mV. The measurements were carried out using compressed powder pellets (diameter of 10 mm and thickness of 1 mm). Gold thin films (diameter of 10 mm) as ion-blocking electrodes were deposited on both faces of the pellets with a quick coater (Quick coater SC-701; Sanyu Electron). Each pellet was sealed in a laminate-type pouch cell to prevent air exposure.

The electronic conductivity was measured using the DC polarization technique. The sample powders were pressed at 360 MPa, and gold current collectors were used to cover the surfaces of the pellets. Each pellet was sealed in a laminate-type pouch cell. The data were collected using a potentio/galvanostat (1287, Solartron) with the applied DC voltage of 0.16 V at room temperature.

The densities of the powder-compressed pellets (d_1) were calculated from the weight and volume of the pellets, and those of the powders (d_2) were measured using a gas pycnometer (AccuPyc II 1340; Shimadzu). The relative density was defined as d_1/d_2. The microstructures of the cross-sections of the pellets were observed *via* scanning electron microscopy (SEM) (JSM-6610A; JEOL).

Cyclic voltammetry was conducted to investigate the electrochemical properties of the prepared Na_3BS_3 glass electrolyte. A composite electrode (80 mg) with $Na_{15}Sn_4$ (80 wt%) and Ketjen Black (KB, 20 wt%) was used as a counter electrode,[17] and a stainless-steel rod was used as a working electrode. The potential sweep was performed between −0.5 V and 5.0 V with a scanning rate of 5.0 mV min^{-1} at 60 °C.

All-solid-state cells were constructed as follows. The Na_3BS_3 glass powder (80 mg) was used as the solid electrolyte. A composite (2.7 mg) of TiS_2 (99%; Kojundo Chem., 40 wt%) and the electrolyte (60 wt%) was used as the positive electrode, and the composite of $Na_{15}Sn_4$–KB (30 mg) was used as the negative electrode. The prepared all-solid-state cells were charged and discharged at 60 °C in the voltage range from 1.2 to 2.4 V at 0.038 mA cm^{-2} under an Ar atmosphere. CV and charge–discharge measurement for the all-solid-state cells were using a potentio/galvanostat device (Bio-logic, VMP-3).

3. Results

Fig. 1 shows the XRD patterns of the Na_3BS_3 crystalline, glassy, and glass–ceramic samples. The XRD pattern of crystalline Na_3BS_3 was the same as that reported for Na_3BS_3 (ICSD: 411608, monoclinic structure[18]). From Na_2S, B, and S as starting materials, crystalline Na_3BS_3 was successfully synthesized by a conventional solid-phase reaction. The crystal was then mechanochemically treated, and the obtained sample showed a halo XRD pattern and an endothermic change attributable to the glass transition at 175 °C (T_g) on the DTA curve, as shown in Fig. 2. The glassy Na_3BS_3 electrolyte was then obtained by a two-step process: synthesis of crystalline Na_3BS_3 from Na_2S, B, and S and amorphization of the crystal. By using this two-step process, the glass-forming region of sodium thioborates was determined. As shown in Fig. S1 (ESI†), the XRD pattern attributable to Na_2S as a starting reagent was observed at compositions of $x = 0.76$ and higher for the $xNa_2S{\cdot}(1-x)B_2S_3$ samples. Glassy electrolytes were prepared in the range of $0.33 \leq x \leq 0.75$ in this study. The glass composition with the highest Na content, $x = 0.75$, corresponds to the *ortho*-thioborate Na_3BS_3.

The Na_3BS_3 glass was heated at 200 or 300 °C corresponding to the exothermic peaks in the DTA curve, as shown in Fig. 2. After heating at 200 °C, a new metastable phase was observed. The XRD pattern was similar to that of the reported monoclinic Na_3BS_3 phase, which is thermodynamically stable, but the new phase was indexed to a higher symmetry. The detailed structural analysis is discussed later. After heating at 300 °C, the glass–ceramic showed almost the same XRD pattern as that of the monoclinic Na_3BS_3 phase.

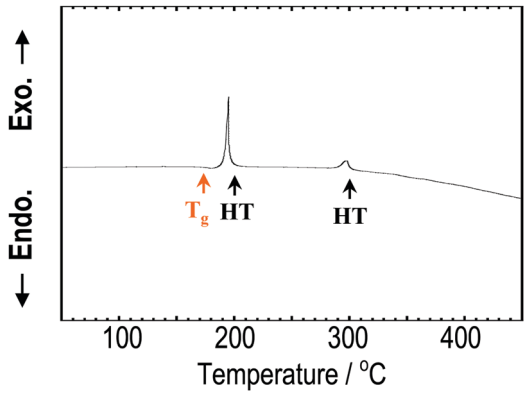

Fig. 2 DTA curve of Na_3BS_3 glass. The orange arrow shows the glass transition temperature, and the two black arrows show the heat-treatment temperatures employed to prepare the glass–ceramics.

The local structure of the Na_3BS_3 samples was analyzed by ^{11}B MAS-NMR measurements and Raman spectroscopy. Fig. 3 shows the ^{11}B MAS-NMR spectra of the Na_3BS_3 solid electrolytes, where the peaks marked with asterisks are spinning side bands. All the samples showed similar spectra. The two resonance peaks between 50 and 70 ppm are attributable to triangular BS_3 units with three-coordinated boron, and the highly symmetrical peaks at 0 and 10 ppm are attributable to tetrahedral BO_xS_{4-x} units with four-coordinated boron.[14] The peaks corresponding to the tetrahedral units were hardly

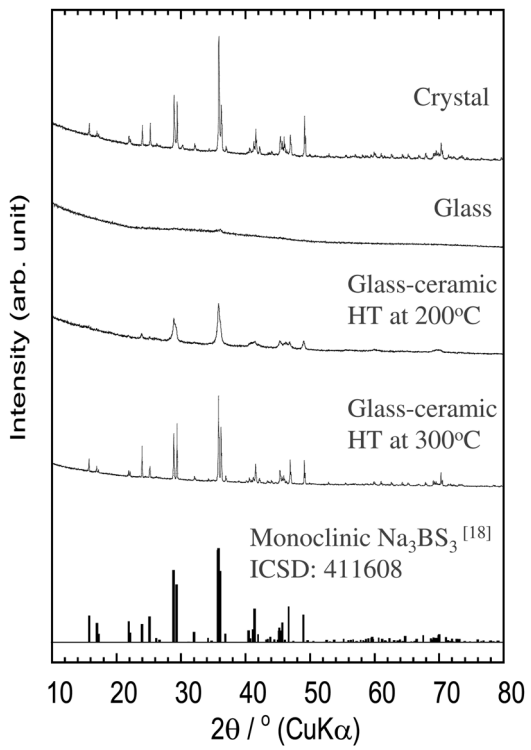

Fig. 1 XRD patterns of Na_3BS_3 solid electrolytes.

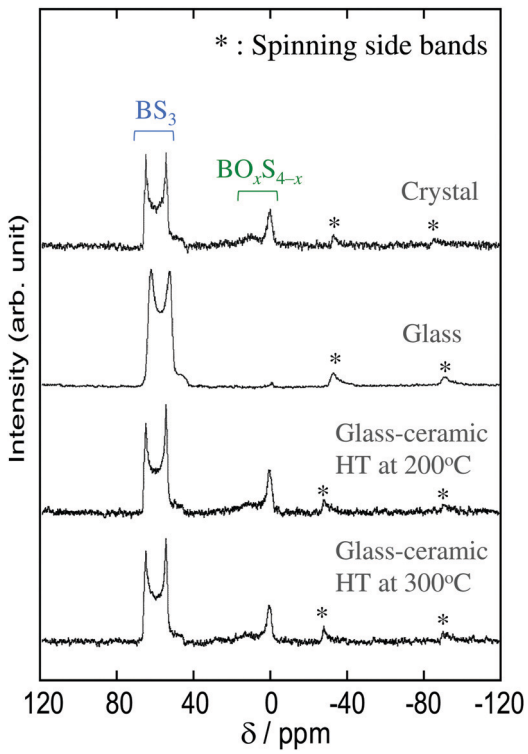

Fig. 3 ^{11}B MAS-NMR spectra of Na_3BS_3 solid electrolytes.

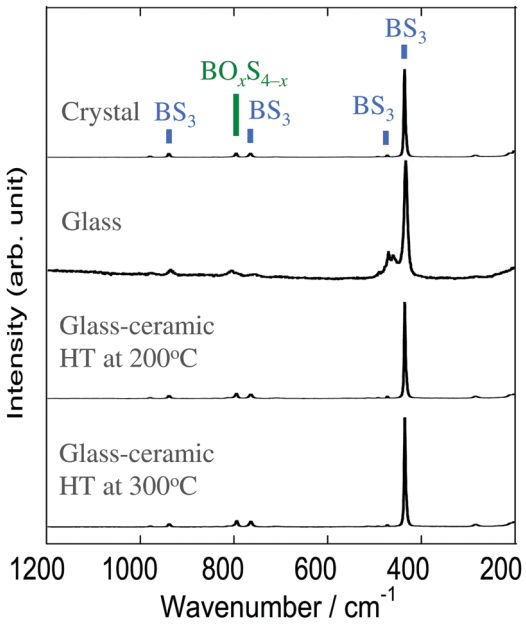

Fig. 4 Raman spectra of Na_3BS_3 solid electrolytes.

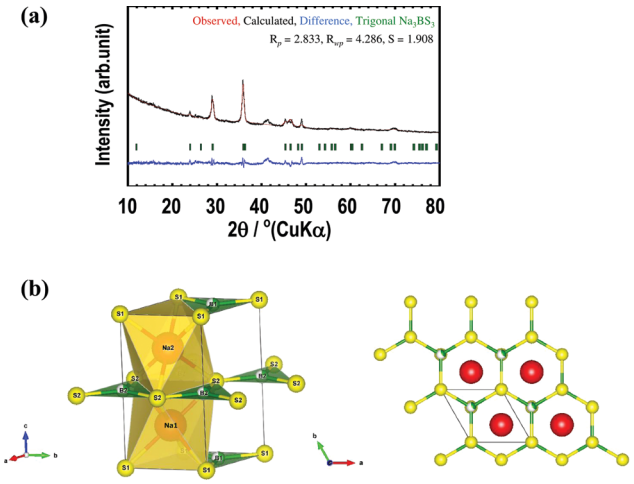

Fig. 5 Crystal structure analysis of Na_3BS_3 metastable phase. (a) X-ray Rietveld refinement profile for the Na_3BS_3 glass–ceramic heated at 200 °C. Solid red and black lines denote the observed and calculated XRD patterns, respectively, and the difference between the curves is shown in blue. The green ticks mark the positions of the reflection allowed by the space group of trigonal Na_3BS_3. (b) Schematic diagram of the crystal structure of trigonal Na_3BS_3. Red, green, and yellow spheres are Na, B, and S, respectively.

observed for the Na_3BS_3 glass, suggesting that the glass mainly consisted of triangular BS_3 units.

The Raman spectra of the Na_3BS_3 samples are shown in Fig. 4. The crystal and glass–ceramics showed similar spectra with a sharp band at 435 cm^{-1} and broad bands at 470, 765, and 940 cm^{-1}, all of which are attributable to triangular BS_3 units.[19] The residual broad band at 795 cm^{-1} is expected to be attributable to tetrahedral BO_xS_{4-x} units since they were detected by ^{11}B MAS-NMR. The spectrum of Na_3BS_3 glass was broader than that of the Na_3BS_3 crystal because of its amorphous nature. Thus, it was concluded that the local structures of all the Na_3BS_3 samples were similar.

Fig. 5(a) shows the Rietveld refinement profile for the Na_3BS_3 glass–ceramic heated at 200 °C. Structural optimization of the new metastable phase resulted in a trigonal crystal structure. The observed and calculated XRD patterns (red and black lines, respectively) were in good agreement, as indicated by their difference spectrum (blue line). Table 1 summarizes the crystallographic parameters including the lattice constants, positions of atoms, thermal factors, and atomic occupancies of the Na_3BS_3 glass–ceramic obtained from the Rietveld refinement. The lattice parameters were a = 3.90 Å, c = 7.42 Å, $\alpha = \beta = 90°$, and $\gamma = 120°$, and the space group was $P3$ (No. 143). The trigonal phase had a higher symmetry than the monoclinic phase of crystalline Na_3BS_3, as shown in Table S1 (ESI†).

Fig. 5(b) and Fig. S2(a) (ESI†) show schematic diagrams of trigonal and monoclinic Na_3BS_3,[18] respectively, generated by the VESTA visualization program. The red, green, and yellow spheres are Na, B, and S, respectively. The major difference between the metastable and stable structures is the distortion of the six-membered ring consisting of B and S atoms. For ease of understanding, Fig. S2(b) (ESI†) shows an image diagram of the monoclinic structure; the Na layers and B–S layers located at different z-positions are shown on the left. Na sites were added to a selected B–S layer. One-third of the B sites of the B–S layers are occupied, and the vacancy sites are shown as gray spheres. In the trigonal structure, the six-membered rings are not distorted because B atoms randomly occupy **1a** or **1b** sites. Conversely, in the monoclinic structure, the B atoms are located at only one of the three sites of the six-membered rings, leading to a distorted framework.

The temperature dependence of the ionic conductivities of the Na_3BS_3 samples is shown in Fig. 6(a), and the Nyquist plot of Na_3BS_3 glass at room temperature is shown in Fig. S3 (ESI†). A semicircle in the higher-frequency region and spike in the lower-frequency region were observed in the Nyquist plot. The insert figure in the Fig. S3 (ESI†) is an equivalent circuit consisting of resistance and constant phase element (CPE). The CPE_2 of the equivalent circuit reflects the capacitance from the Au current collector. The bulk and grain-boundary contributions were not reliably separated and thus the herein reported conductivities were calculated from total resistance R. The glass–ceramic heated at 300 °C had a low ionic conductivity, and thus it was measured only at 106 °C. For the other samples, the temperature dependence of the ionic conductivities obeyed the Arrhenius equation, and thus the activation energies were calculated from the Arrhenius plots. Their ionic conductivities at 25 °C (calculated from the Arrhenius equation) and activation energies are summarized in Table 2; for the glass–ceramic heated at 300 °C, the experimental conductivity determined at 106 °C is listed. The room-temperature ionic conductivity and activation energy of the Na_3BS_3 glass were 1.1×10^{-5} S cm^{-1} and 39 kJ mol^{-1}, respectively. This conductivity is higher than those of Na_3BO_3 glass[13] and Na_3PS_4 glass,[5] as shown in Fig. 6(b). The ionic conductivities at

Table 1 Atomic coordinates of the Na_3BS_3 metastable phase

Phase			Na_3BS_3			
Crystal system			Trigonal			
Space group			*P*3 (No. 143)			
Lattice parameter, volume, *Z*			a = 3.901(1) Å, c = 7.422(1) Å, V = 97.83(1) Å^3 α = 90, β = 90, γ = 120, Z = 1			
Atoms	*x*	*y*	*z*	Site	Occupancy	*B*
Na1	0.6667	0.3333	0.2467(1)	**1c**	1.0000	1.000
Na2	0.6667	0.3333	0.7468(1)	**1c**	1.0000	1.000
S1	0.0000	0.0000	0.0000	**1a**	1.0000	1.000
S2	0.3333	0.6667	0.5000	**1b**	1.0000	1.000
B1	0.3333	0.6667	0.0000	**1b**	0.3333	1.000
B2	0.0000	0.0000	0.5000	**1a**	0.3333	1.000

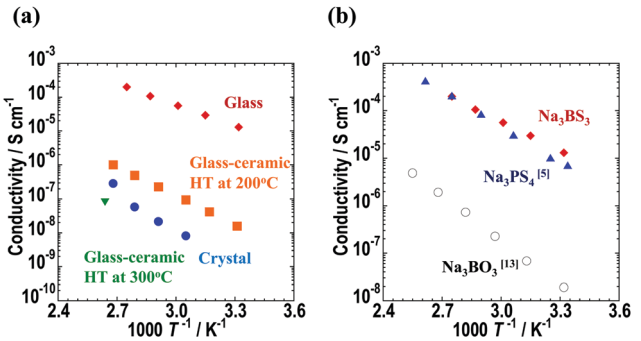

Fig. 6 Temperature dependence of conductivity for (a) Na_3BS_3 glass, glass–ceramics, and crystal electrolytes and (b) Na_3BS_3, Na_3BO_3,[13] and Na_3PS_4,[5] glass electrolytes.

Table 2 Ionic conductivities at room temperature (σ_{25}), activation energies (E_a), densities of pellets (d_1) and powders (d_2), and relative density (d_1/d_2) of Na_3BS_3 solid electrolytes

	σ_{25}/S cm^{-1}	E_a/kJ mol^{-1}	d_1 (g cm^{-3})	d_2 (g cm^{-3})	Relative density (%)
Crystal	3.7 × 10^{-10}	79	1.725	1.996	86.4
Glass	1.1 × 10^{-5}	39	1.824	1.932	94.4
g.c. (HT200 °C)	1.2 × 10^{-8}	55	1.529	1.999	76.5
g.c. (HT300 °C)	8.0 × 10^{-8} (at 106 °C)	—	1.701	2.001	85.0

d_1: density calculated from the volume measured by dimension of the pellet. d_2: density calculated from the volume measured by a gas pycnometer.

25 °C and activation energies of other reported sodium-ion conducting glassy electrolytes are summarized in Table S2 (ESI†).[5,13,14,20,21] The electronic conductivity at room temperature measured *via* DC polarization was 7.6 × 10^{-10} S cm^{-1}, which is five orders of magnitude lower than the ionic conductivity. Thus, the sodium-ion transport number of the Na_3BS_3 glass was almost unity. Fig. S4 (ESI†) shows the room-temperature ionic conductivities and activation energies of the xNa$_2$S·(1 − x)B$_2$S$_3$ (0.33 ≤ x ≤ 0.75) glass electrolytes. In the glass-forming region, Na_3BS_3 glass showed the highest ionic conductivity and the lowest activation energy because of its highest Na content.

The glass showed the highest ionic conductivity among the prepared Na_3BS_3 solid electrolytes. Between the glass–ceramics heated at 200 and 300 °C, the former showed a higher ionic conductivity. Table 2 lists the densities of the powder-compressed pellets (d_1) and powders (d_2) and the relative densities (d_1/d_2) of the Na_3BS_3 solid electrolytes. After heat treatment, the glass–ceramics showed lower relative densities than the glass because of crystal precipitation. The Na_3BS_3 glass pressed at 360 MPa showed the highest relative density of 94%, which is higher than that of Na_3BO_3 glass (88%) pressed at 720 MPa.[13] This is related to the fact that the sulfide ion has a larger polarizability than the oxide ion. The high relative density means that the Na_3BS_3 glass has a favorable formability. Of other sulfide-based solid electrolytes, the relative density of Na_3PS_4 glass pressed at 360 MPa was 94%,[6] indicating that the Na_3BS_3 glass has a similar formability. Fig. 7 shows an SEM image of the fractured cross-section of the powder-compressed pellet of the Na_3BS_3 glass, indicating that the glass showed good formability.

Cyclic voltammetry was conducted to investigate the electrochemical properties of the Na_3BS_3 glass. Fig. S5(a) (ESI†) shows cyclic voltammogram of an all-solid-state two-electrode cell using the Na_3BS_3 glass electrolyte. Stainless-steel and $Na_{15}Sn_4$–KB were used as working and counter electrodes, respectively. The potential sweep was performed with a scanning rate of 5.0 mV min^{-1} at 60 °C. Reduction and oxidation currents attributable to sodium deposition and dissolution

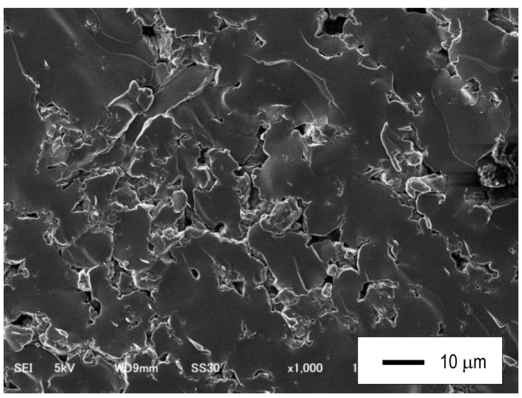

Fig. 7 Cross-sectional SEM image of the Na_3BS_3 glass.

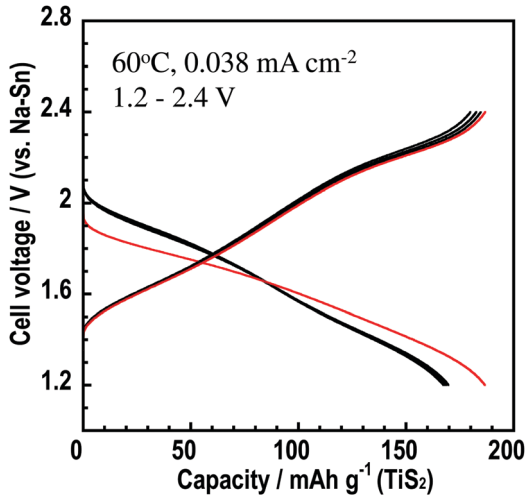

Fig. 8 Charge–discharge curves of the all-solid-state cell $Na_{15}Sn_4$/Na_3BS_3 glass/TiS_2 cell at 60 °C and a current density of 0.038 mA cm^{-2} in the potential range of 1.2–2.4 V.

were observed at around 0 V *versus* the counter electrode, and no remarkable oxidation current was observed up to 5.0 V. This suggests that the Na_3BS_3 glass has a wide electrochemical window of 5.0 V. Fig. S5(b) (ESI†) shows the cross-sectional SEM image of the cell after cyclic voltammetry. The working electrode of stainless steel was removed from the cell and two layers of Na_3BS_3/$Na_{15}Sn_4$–KB were observed. A close contact at the interface between the two layers was maintained and unfavourable deterioration for the interface was not observed.

The Na_3BS_3 glass was used as an electrolyte in an all-solid-state cell. Fig. 8 shows the initial five charge–discharge curves of the all-solid-state $Na_{15}Sn_4$/Na_3BS_3 glass/TiS_2 cell. The cell was operated as a sodium secondary battery at 60 °C, where the conductivity of the Na_3BS_3 glass was 5.8×10^{-5} S cm^{-1}, and showed an initial charge capacity of 190 mA h g^{-1}. A capacity of approximately 170 mA h g^{-1} was retained from the second to the fifth cycle, suggesting that Na_3BS_3 glass is adopted as a solid electrolyte for all-solid-state cells manufactured only by pressing.

4. Discussion

Compared with the ionic conductivities of the glass–ceramics, the glass–ceramic heated at 200 °C showed higher ionic conductivity than that heated at 300 °C. This was due to the obtaining of the metastable phase with a higher ionic conductivity than the stable phase. The activation energy of metastable phase was 55 kJ mol^{-1}. That of stable phase of glass–ceramic was not measured, but the activation energy of the Na_3BS_3 crystal which showed the same stable phase was 79 kJ mol^{-1}. It suggests that the activation barrier to ion conduction of metastable phase was smaller than that of stable phase due to the higher symmetry of the structure.

The ionic conductivity of the glass was higher than those of the glass–ceramics and crystal because of the random structure and free volume for ionic conduction. Moreover, this conductivity is higher than that of Na_3PS_4 glass.[5] These relative densities were same value (94%).[6] Thus, the difference between these ionic conductivities is not caused by their formabilities. The activation energy of Na_3BS_3 glass was 39 kJ mol^{-1}, which was lower than that of Na_3PS_4 glass (47 kJ mol^{-1}).[5] This suggests that the activation barrier to ion conduction of the Na_3BS_3 glass with planar triangular BS_3 units is smaller than that of the Na_3PS_4 glass with tetrahedral PS_4 units. It was also found that the mean atomic volumes of the Na_3BS_3 glass and Na_3PS_4 glass were calculated using the powder densities of these glasses (1.932 g cm^{-3} of Na_3BS_3 glass and 2.002 g cm^{-3} of Na_3PS_4 glass). The mean atomic volume of the Na_3BS_3 glass is 13.0 cm^3 mol^{-1}, which is smaller than that of the Na_3PS_4 glass (14.2 cm^3 mol^{-1}). It suggests the high ionic conductivity of Na_3BS_3 glass is related with its larger packing density compared to the Na_3PS_4 glass.

5. Conclusions

The Na_3BS_3 glassy electrolyte was prepared and its electrical and electrochemical properties were examined for the first time. The new metastable Na_3BS_3 phase with a trigonal structure was formed as a primary phase by crystallization of the Na_3BS_3 glass, and showed a higher ionic conductivity than the previously reported monoclinic Na_3BS_3 phase. The room-temperature ionic conductivity and activation energy of the Na_3BS_3 glass were 1.1×10^{-5} S cm^{-1} and 39 kJ mol^{-1}, respectively and its crystallization decreased conductivity. In addition, the Na_3BS_3 glass showed a favorable formability. The all-solid-state cell operated with the prepared glass as the electrolyte exhibited a reversible capacity of approximately 170 mA h g^{-1} during five charge–discharge cycles at 60 °C. It is concluded that the Na_3BS_3 glass with triangular structural units has appropriate properties as a solid electrolyte for application to all-solid-state sodium batteries. The results of this study extend research toward designing multi-component sulfide electrolytes with triangular BS_3 structural units and contribute to the development of solid electrolytes for all-solid-state batteries.

Conflicts of interest

There are no conflicts to declare.

Acknowledgements

This work was supported by the Element Strategy Initiative of MEXT, Grant Number JPMXP0112101003, and JSPS KAKENHI Grant Numbers 18H01713 and 19H05816.

References

1 B. L. Ellis and L. F. Nazar, *Curr. Opin. Solid State Mater. Sci.*, 2012, **16**, 168.
2 K. B. Hueso, M. Armand and T. Rojo, *Energy Environ. Sci.*, 2013, **6**, 734.

3 H. Pan, Y.-S. Hu and L. Chen, *Energy Environ. Sci.*, 2013, **6**, 2338.
4 X. Lu, G. Xia, J. P. Lemmon and Z. Yang, *J. Power Sources*, 2010, **195**, 2431.
5 A. Hayashi, K. Noi, A. Sakuda and M. Tatsumisago, *Nat. Commun.*, 2012, **3**, 856.
6 M. Nose, A. Kato, A. Sakuda, A. Hayashi and M. Tatsumisago, *J. Mater. Chem. A*, 2015, **3**, 22061.
7 A. Banerjee, K. H. Park, J. W. Heo, Y. J. Nam, C. K. Moon, S. M. Oh, S. T. Hong and Y. S. Jung, *Angew. Chem., Int. Ed.*, 2016, **55**, 9634.
8 H. Wang, Y. Chen, Z. D. Hood, G. Sahu, A. S. Pandian, J. K. Keum, K. An and C. Liang, *Angew. Chem., Int. Ed.*, 2016, **55**, 8551.
9 L. Zhang, D. Zhang, K. Yang, X. Yan, L. Wang, L. Mi, B. Xu and Y. Li, *Adv. Sci.*, 2016, **3**, 1600089.
10 M. Duchardt, U. Ruschewitz, S. Adams, S. Dehnen and B. Roling, *Angew. Chem., Int. Ed.*, 2018, **57**, 1351.
11 Z. Zhang, E. Ramos, F. Lalère, A. Assoud, K. Kaup, P. Hartman and L. F. Nazar, *Energy Environ. Sci.*, 2018, **11**, 87.
12 A. Hayashi, N. Masuzawa, S. Yubuchi, F. Tsuji, C. Hotehama, A. Sakuda and M. Tatsumisago, *Nat. Commun.*, 2019, **10**, 5266.
13 K. Suzuki, Y. Nakamura, N. Tanibata, A. Hayashi and M. Tatsumisago, *J. Asian Ceram. Soc.*, 2016, **4**, 6.
14 D. Larink, H. Eckert and S. W. Martin, *J. Phys. Chem. C*, 2012, **116**, 22698.
15 S. W. Martin and D. R. Bloyer, *J. Am. Ceram. Soc.*, 1990, **73**, 3481.
16 F. Izumi and K. Momma, *Solid State Phenom.*, 2007, **130**, 15.
17 A. Hayashi, K. Noi, N. Tanibata, M. Nagao and M. Tatsumisago, *J. Power Sources*, 2014, **258**, 420.
18 J. Kuchinke, C. Jansen, A. Lindemann and B. Krebs, *Z. Anorg. Allg. Chem.*, 2001, **627**, 896.
19 M. Royle, J. Cho and S. W. Martin, *J. Non-Cryst. Solids*, 2001, **279**, 97.
20 I. A. Sokolov, V. N. Naraev and A. A. Pronkin, *Glass Phys. Chem.*, 2000, **26**, 588.
21 M. Nose, A. Kato, A. Sakuda, A. Hayashi and M. Tatsumisago, *J. Mater. Chem. A*, 2015, **44**, 22061.